Comparative study of oxide dissolution modeling in secondary steelmaking slags

N Preisser[1]*, and S K Michelic*[2]

1.PhD-candidate, Christian Doppler Laboratory for Inclusion Metallurgy in Advanced Steelmaking, Leoben, Austria, A-8700. Email: nikolaus.preisser@unileoben.ac.at
2.Full-professor, Christian Doppler Laboratory for Inclusion Metallurgy in Advanced Steelmaking, Leoben, Austria, A-8700. Email: susanne.michelic@unileobane.ac.at

Keywords: Non-metallic Inclusions, Dissolution, Slag, Dissolution-Model, Diffusion, stationary Interface

ABSTRACT

For certain applications, steels have to feature a very distinct and well-defined level of cleanness in terms of the number and composition of non-metallic inclusions. Therefore, one crucial aspect of steelmaking is removing and controlling said non-metallic inclusions during the process. Particle removal during ladle refining comprises 3 stages, namely 1.) Flotation, 2.) Transport through the steel/slag interface, and 3.) Dissolution of the particle in the slag. Only if all three stages are completed the particle can be considered as fully removed from the steel melt which, in turn, leads to the slag being one of the most influential parameters for inclusion removal and control. Depending on the composition of the particles and the slag, the dissolution can be controlled by different mechanisms. This study focuses on the diffusion-controlled dissolution of solid oxidic particles in slags. For this, a model of particle dissolution has been developed. For modeling diffusion, either the differential equation following Fick's second law can be solved, or an analytical solution to this equation valid for stationary interfaces can be used. Both approaches allow for calculations of concentration profiles of the dissolving species in surrounding slag. From this, the mass flux can be derived, which finally leads to calculating the boundary layer velocity due to considerations of mass balance. In this work, both methods as well as results of dissolution experiments using High Temperature Confocal Scanning Laser Microscopy are compared. This research aims to provide a framework for diffusion-based dissolution modeling in further expanding the understanding of particle dissolution in secondary metallurgy.

INTRODUCTION

The possible applications of steel and steel products are constantly rising. Much of this is due to the fact that enhanced steel cleanness is improving the mechanical, chemical and physical properties of the steel as shown by Garrison and Wojcieszynski (2007) and Chen et al (2019). One of the most essential aspects for steel cleanness is the secondary metallurgy in the steel plant especially the interaction of the steel with the slag phase. And as Sridhar and Cramb (2003) state, slags heavily influence the steel cleanness as the slag's properties are linked to multiple processes essential for steel cleanness. As non-metallic inclusions (NMI) are similar in composition to secondary metallurgical slags, there is a tendency towards chemical equilibrium between particles and slag, and the chemical composition of NMIs can be influenced. Moreover, the slag's surface tension and viscosity is important for the transition of NMIs from the steel to the slag-phase as shown by Jimbo, Chung and Cramb (1996). And lastly, slags are responsible for the dissolution and, therefore the ultimate removal of NMIs from the system, as stated by Valdez, Shannon and Sridhar (2006) and Lee et al (2001). only if the NMIs can be transported to the steel-slag interface by mechanisms like flotation, move through this interface due to advantageous wetting conditions and surface tensions, and are then dissolved in the slag promptly to avoid re-entrapment in the steel, the particles can be considered entirely removed. For most applications especially hard and non-deformable NMIs are detrimental. Furuya, Abe and Matsuoka (2003) found that this is because especially with dynamic loads and many load cycles cavities can form around particles, which are not as deformable as the surrounding steel matrix. These cavities can then be the origin of cracks and lead to critical failure of the material. Therefore, it is of interest to gain a better understanding of the mechanisms which are involved in the removal of such particles from the steel melt to ensure the highest possible steel cleanness, avoid fracture of the material, and enable smaller diameters, which in turn will lead to economic and ecological benefits. This work focuses on the last step of particle removal, the dissolution of NMIs in slags. Solid oxide particles like Al2O3, which are particularly harmful to the mechanical properties of steel, are studied. This is done by simulations of particle dissolution and experimentally, using high temperature confocal scanning laser microscopy (HT-CSLM), which allows in-situ investigation of particle dissolution in slags at steelmaking temperatures.

From the work of Levenspiel (1999.), it is clear that dissolution can be explained by different mechanisms that lead to very distinct dissolution curves. Suppose the dissolution is for example limited by some kind of chemical reaction between the particle and the matrix in which it dissolves. In that case, the dissolution takes place linearly, where the speed of dissolution can be directly found from the speed of the chemical reaction. In contrast, this work focuses on dissolution purely governed by the diffusion of solid particles into the liquid slag as Huo et al. (2022) indicate that this shows promising results for the dissolution of solid oxide particles in steelmaking slags.

DESCRIPTION OF THE MODEL

The dissolution behaviour is portrayed in this work, assuming a stationary interface between the particle and the slag phase. According to Guo et al (2017) this approach models dissolution behaviour more accurately as the alternative to invariant field or reverse growth approximations. For this model, the interface where mass is transferred from the solid particle to the liquid slag is fixed at a position equal to the initial radius of the dissolving particle. Using this approach, the following calculations are simplified, as a homogeneous distance between spatial steps is used for a finite differences method. In contrast, a moving interface would lead to varying distances between calculation points.

For the diffusion simulation using this method, several parameters have to be provided. Parameters describing the system's spatial layout include the initial radius of the spherical particle, the width of the boundary layer, and the number of spatial steps where calculations should be performed. The boundary layer describes a zone surrounding the solid particle where diffusive processes can occur. Outside of this boundary layer, the slag composition is assumed to be unchanged over the whole process of dissolution. All spatial steps where calculations of the concentration profile will be performed lie within this boundary layer between the particles' initial surface at time 0 and the edge of the boundary layer. A visual representation of the spatial layout of this simulation is represented in FIG 1.

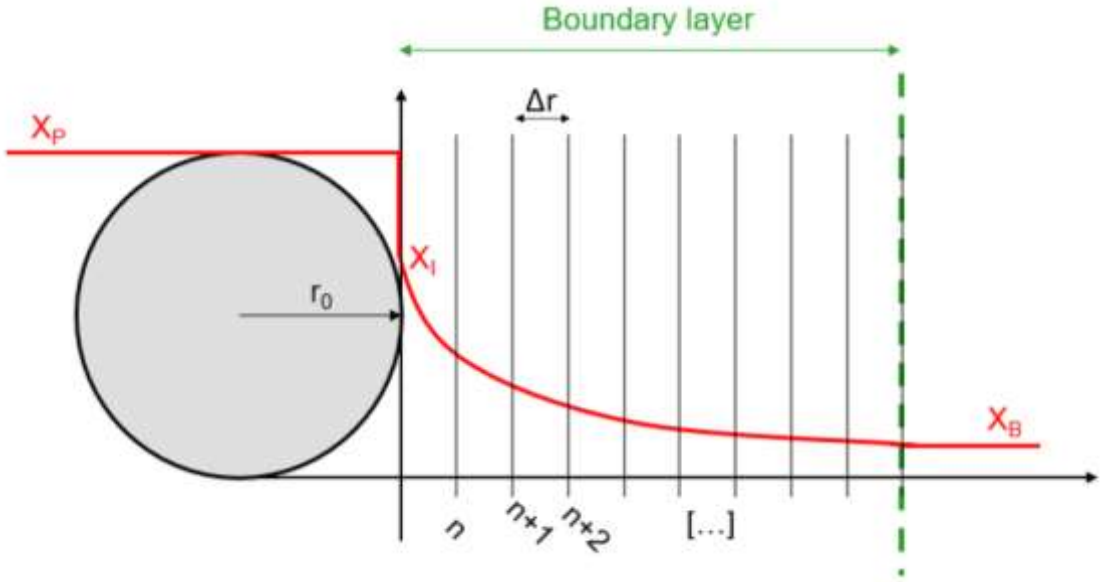

FIG 1 - Spatial layout of the diffusion model.

Additionally, chemical information about the system has to be provided, like the composition of the particle regarding the dissolving species as the dimensionless weight percentage x_P (in this case, x_P=1 as a homogeneous particle of one species is assumed), the weight percentage x_B of the dissolving species in the slag in the bulk zone (initial composition of the slag), as well as the weight percentage of the dissolving species in the slag saturated with the dissolving species (ie this is assumed to be the composition of the slag directly at the interface between particle and slag). The weight percentage of the dissolving species in the saturated slag is calculated via the thermodynamic calculation software FactSage 8.3 using the Equilib module. Lastly, the diffusion coefficient has to be provided to calculate the concentration profile around the dissolving particle at all times. The spatial stepsize can be calculated from the boundary layer thickness and the number of desired spatial steps. From this and the diffusivity the critical temporal stepsize can be calculated following Equation 1 were Δt is the length of the temporal timestep Δr is the size of the spatial step and D is the diffusion coefficient.

$$\Delta t = \frac{\Delta r^2}{2D} \qquad \text{(Equation 1)}$$

With the number of necessary timesteps and the defined number of spatial steps, the corresponding space and time matrices for the simulation of the concentration field around the particle can be set. The initial conditions for the concentration profile are set so that for all timesteps, the mass percentage of dissolving species at the interface is x_I. At the same time, it is x_B at any other spatial step. Additionally, the temporal derivative of the concentration field is set to be 0 at all spatial steps initially. The temporal derivative of the concentration field can be calculated for each timestep following Equation 2, as stated by Ogris and Gamsjäger (2022). Where x_{i-1}, x_i, and x_{i+1} are the mass fractions of the dissolving species at a spatial position at different calculation times. The concentration field of the next timestep then follows as the sum of the concentration field of the current timestep and the calculated temporal derivative multiplied by the length of the timestep. Now, the spatial derivative of the concentration profile can be calculated at each spatial step for each timestep as seen in Equation 3. From this, the mass flux is calculated using Fick's second law of diffusion given in Equation 4 where J is the mass flux and $\dot{x}$ is the spatial derivative of the concentration profile. As the dimensionless mass percentage was used for the calculation of the concentration profile instead of actual concentrations, this flux would have to be multiplied with the slags density in order to resemble actual mass flux with unit $kgm^{-2}s^{-1}$. Due to this simplification the actual unit of this flux of weight fraction is ms^{-1} Now the reduction in diameter of the particle can be calculated for each timestep. This is performed using a mass balance equation called 'Stefan's interface condition' after Slovenian scientist Jozef Stefan as found in Glicksman (2000). This mass balance is given in Equation 5. On the left hand side, the mass leaving the interface is given as the product of the interface area multiplied by the mass flux at the interface $J(R_0)$, the length of the timestep Δt, and the slags density. On the right hand side, the respective difference in the spherical particle volume is multiplied by the particle density. For this simulation, the density of the solid particle and the density of the slag at the interface are assumed to be the same, which allows for simplification and rearrangement of Equation 5 to determine the radius of the particle in the next time step. This is shown in Equation 6.

$$\frac{\Delta x}{\Delta t} = D\left(\frac{x_{i-1} + x_{i+1} - 2x_i}{\Delta r^2} + \frac{x_{i+1} - x_{i-1}}{r_i \Delta r}\right) \quad \textit{(Equation 2)}$$

$$\dot{x} = \frac{\Delta x}{\Delta r} = \frac{x_{n+1} - x_n}{\Delta r} \quad \textit{(Equation 3)}$$

$$J = -D\dot{x} \quad \textit{(Equation 4)}$$

$$4\pi R_0^2 J(R_0)\, \Delta t\, \rho = \frac{4}{3}\pi \left(r_i^3 - r_{i+1}^3\right)\rho \quad \textit{(Equation 5)}$$

$$r_{i+1} = \sqrt[3]{\left(r_i^3 - 3\, J(R_0)\right) \Delta t\, R_0^2} \quad \textit{(Equation 6)}$$

PARAMETER ANALYSIS

The impact of changes of initial parameters is presented and discussed. This is necessary to further understand the models' capabilities and restrictions for further application. In FIG 2 the dissolution curves of various simulations are shown. In subfigure FIG 2 a), the only difference in parameters is the number of spatial steps chosen between the interface and the outer edge of the boundary layer. As absolute values are plotted, it can be seen that with an increasing number of calculation points, the curve is shifted to slightly faster dissolution times. At the same time, the difference between simulations gets smaller as the number of spatial steps increases. Therefore, it can be assumed that the result of the simulation converges, and at some stage, increasing the number of calculation points does not result in significantly more accurate results.

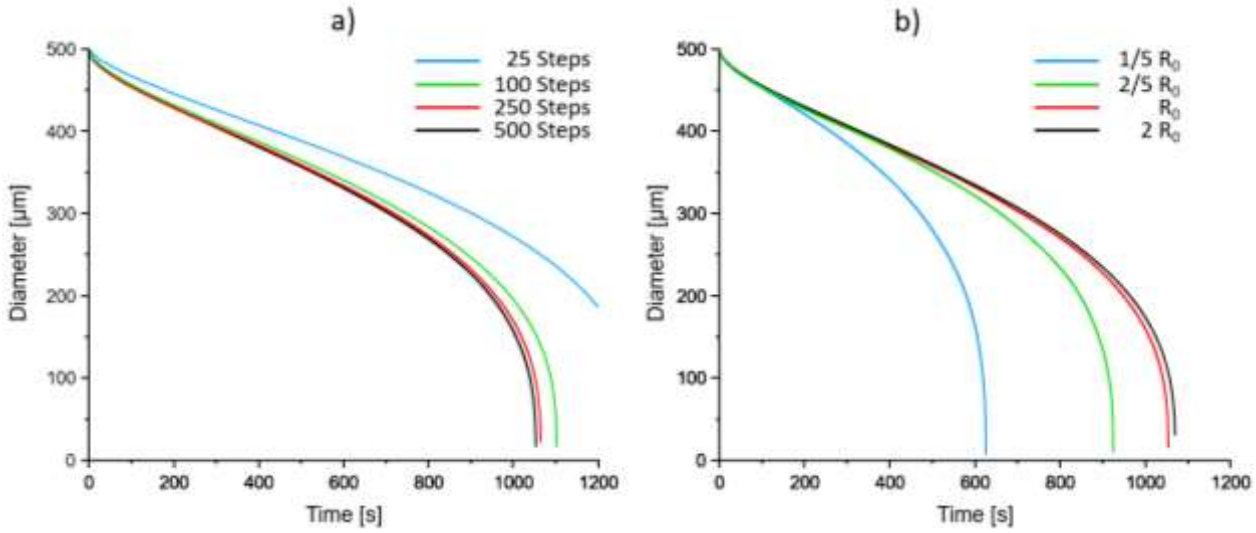

FIG 2 - Variation of number of spatial steps and boundary layer thickness

In Subfigure FIG 2 b), the impact of the thickness of the boundary layer is shown. This parameter heavily influences the shape of the concentration profile, where smaller values lead to steeper gradients in concentration as the zone where an unchanged composition of the bulk medium is assumed moves closer to the interface between slag and particle. Therefore, smaller values for the boundary layer thickness result in faster particle dissolution. In this example, the slowest dissolution is achieved when the boundary layer thickness is double the initial radius of the particle. With decreasing boundary layer thickness, the dissolution of the particle rapidly speeds up, as the last line representing a boundary layer thickness of one fifth of the initial radius of the particle, shows much faster dissolution. Lastly, the influence of different diffusion coefficients was analysed with fixed amounts of spatial steps, boundary layer thickness, and initial radius of the particle. In FIG 3 a) it can be seen that dissolution is faster with higher values for the diffusion coefficient, as would be expected. The normalized dissolution curves are depicted in FIG 3 b). Normalized dissolution curves are derived by dividing particle diameters by their initial values at time zero, and time by the total dissolution time. This normalization technique allows for a direct comparison of dissolution behavior across different scenarios, independent of specific particle sizes or dissolution durations. Here it is clear that a change in diffusion coefficient does not affect the general shape of the dissolution curve, as the normalized dissolution curves for all values for the diffusion coefficient are congruent. This observation suggests that while the diffusion coefficient influences the rate at which dissolution occurs, it does not alter the overall kinetics of the dissolution process.

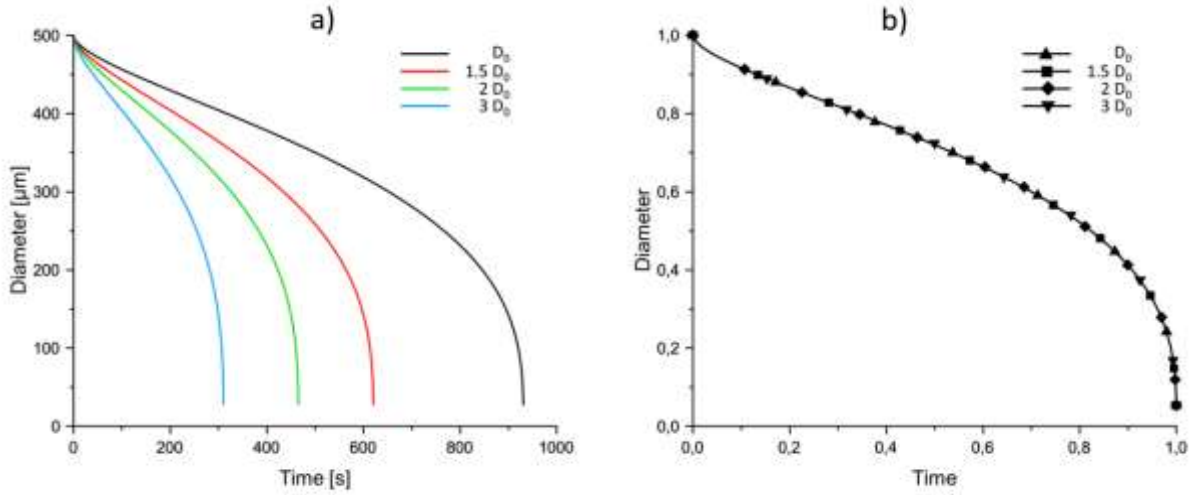

FIG 3 - Influence of changes in diffusion coefficient

DESCRIPTION OF HT-CSLM AND EXPERIMENTAL SETUP

For model validation, dissolution experiments have been conducted using high temperature confocal scanning laser microscopy (HT-CSLM). With this, the dissolution of particles in slags can be observed in-situ and the dissolution curves can be gathered directly. The experimental setup has already been widely discussed in previous work by Michelic et al (2016) as well as Feichtinger, Michelic, Kang and Bernhard (2014) and will not be presented in detail. For validation of the model, a specific combination of particle, slag, and temperature with a known diffusion coefficient has been selected from the literature. The slag composition is given in TABLE 1. The selection of slag is crucial for the analysis of the dissolution as it is paramount that the slag is transparent for the laser with a wavelength of 405 nm. Therefore, slags without tainting constituents like FeO or MnO should be used. The particles used for the dissolution experiment are synthetic Al_2O_3 particles with nearly perfect spherical geometry and an initial particle diameter of 500 µm. The slag is heated together with the particle to 1500°C. The particle is then manually tracked. The software directly logs the time and individual temperature. The corresponding particle diameter is gathered by extracting single frames from the video data afterwards and measuring the particle's dimensions. From this dissolution curves of diameter over time can be plotted. As time zero of dissolution, the time is chosen at which the experimental temperature of 1500°C is reached. Dissolution, which occurs before this point in time, is disregarded. Third-order polynomial smoothing of the data is performed using the SimpleFit Module of OriginPro, Version 2023. OriginLab Corporation, Northampton, MA, USA. The data of both experiments are comparably close, which results in nearly identical dissolution curves after polynomial fitting. The total dissolution is achieved after approximately 900 seconds in both experiments. From both data sets it can be derived that the dissolution rate at the beginning as well as at the end of the dissolution is faster. This behaviour is quite common and must be expected if diffusion is assumed to be the limiting factor of dissolution. This is because of a steeper concentration gradient in the beginning of dissolution and a favorable relation of the particle's surface area to its volume.

TABLE 1 - Slag composition

Name	**SiO_2 [wt.%]**	**CaO [wt.%]**	**Al_2O_3 [wt.%]**	**MgO [wt.%]**
Slag 1	49.56	32.42	11.16	6.86

COMPARISON OF SIMULATION AND EXPERIMENTAL RESULTS

For validation of the simulation, the experimental results are compared with the dissolution curves calculated by the model using the presented stationary interface approach of dissolution modeling. The boundary layer thickness for the calculation was chosen to be 500µm, which is double the synthetic particle's initial radius. The diffusion coefficient was set to $4.56*10^{-11,}$ as found in the work of Burhanuddin et al (2022) for the diffusion of Al_2O_3 in the specific slag used in the HT-CSLM experiments. As pure Al_2O_3 particles are dissolved, the mass fraction of Al_2O_3 of the particle is 1. The mass fraction of Al_2O_3 in the bulk slag is 0.1119 and the mass fraction of Al_2O_3 in the saturated slag is 0.3970, as calculated by Factsage. For a relatively short computation time, 200 spatial steps were chosen for calculations between the interface and the outer edge of the boundary layer. With these parameters, a total dissolution time of approximately 600 s was calculated. At first glance, this would lead to the conclusion that the simulation does not describe the dissolution well, as this value is about a third lower than the dissolution time gathered from the HT-CSLM experiments. But by closer comparison, it becomes apparent that this discrepancy in dissolution time arises mainly in the second half of the dissolution when the diameter of the particles gets smaller. In contrast, the dissolution rate at the beginning of the dissolution is predicted with high accuracy. While the experimental data only shows a slight pick-up in the dissolution speed, the model leads to a drastic increase in dissolution rate to the point where the particle is expected to dissolve almost instantaneously after a decrease in diameter of about 75%. In FIG 4 the data of both dissolution experiments and the calculated dissolution curve from the model are depicted.

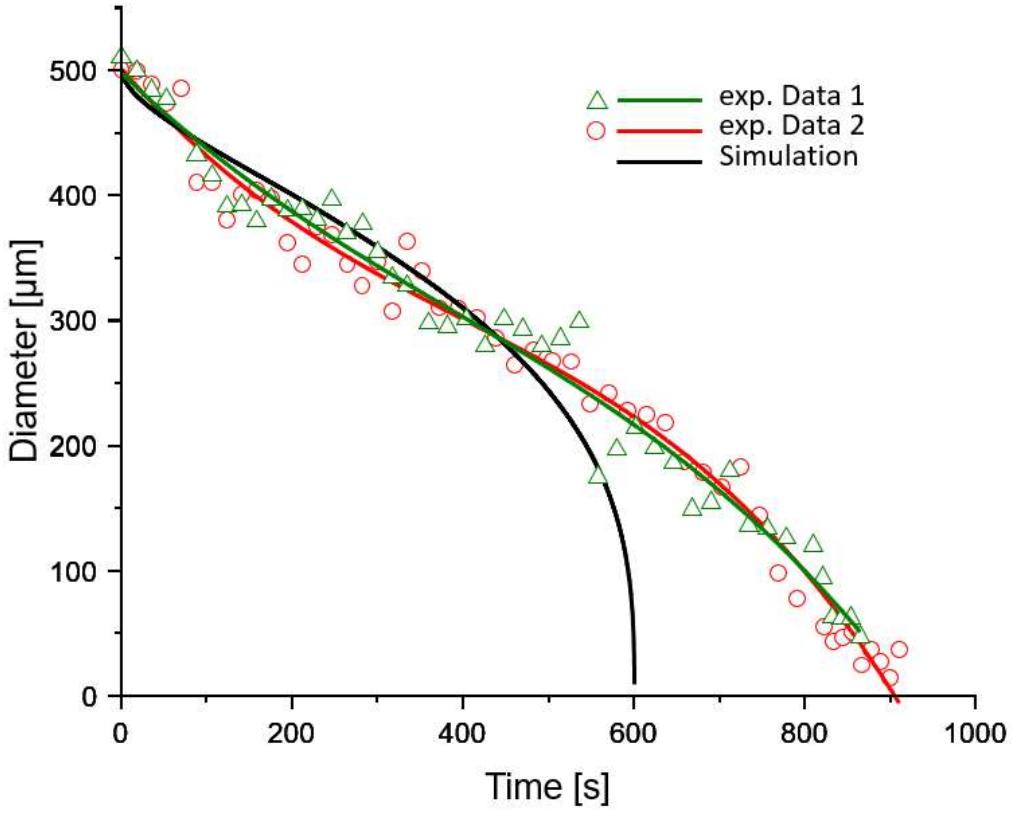

FIG 4 - Comparison of experimental results of dissolution curves and simulated dissolution curve

DISCUSSION

In this work, a model for the simulation of diffusion-based dissolution of solid particles in liquid slags has been developed. The model follows a stationary interface approach, where for the sake of calculating the concentration profile around the particle and mass balance considerations, the interface is considered as not moving. This aids the calculation as the vectorized space for finite differences methods is homogeneous, where, in contrast, a moving interface would lead to inhomogeneous distances between nodal points of calculation and the concentration profile would need to be recalculated after each timestep as opposed to being calculated once upfront. For comparison, dissolution experiments have been conducted using HT-CSLM, where the dissolution of a synthetic particle in an experimental slag can be observed in-situ at steelmaking temperatures. Dissolution rates of the experiments and the simulation are in good agreement at the beginning of the dissolution but deviate towards smaller diameters as the simulation predicts a faster pick-up in dissolution speed. This is believed to be an effect of the stationary interface approach, as the surface through which mass flux is assumed stays constant as the surface area of the initial particle, whereas in reality this also decreases in size throughout the dissolution. To clarify this effect, the ratio of surface area for mass flux and particle volume can be calculated for both a moving and a stationary interface approach. In Equation 7 this ratio is expressed for the case of a moving interface as γ_M. Equation 8 states the same ratio γ_S but for the case of a stationary interface.

$$\gamma_M = \frac{A}{V} = \frac{4\,\pi\,r^2}{\frac{4}{3}\,\pi\,r^3} = \frac{3}{r} \qquad \textit{(Equation 7)}$$

$$\gamma_s = \frac{A}{V} = \frac{4\,\pi\,R_0^2}{\frac{4}{3}\,\pi\,r^3} = \frac{3\,R_0^2}{r^3} \qquad \textit{(Equation 8)}$$

From these ratios, it is clear that with decreasing values of r the ratio γ_S will increase much faster than the ratio γ_M. This could in turn explain the difference between the experimental results and the simulation of dissolution in later stages of the dissolution process, as the mass flux through the surface area becomes overpronounced with decreasing particle diameters. To better understand the scope of this discrepancy between the different models, a critical radius can be calculated, which

marks the radius at which the stationary interface approach theoretically overtakes the moving interface approach, given the concentration field would be the same for both calculations. This can be done by comparing the first derivative of both surface-to-volume ratios, which are shown in Equation 9 and Equation 10.

$$\dot{\gamma}_M = -\frac{3}{r} \qquad \textit{(Equation 9)}$$

$$\dot{\gamma}_S = -\frac{9\,R_0^2}{r^4} \qquad \textit{(Equation 10)}$$

If these derivatives are compared, a critical value r_{crit} can be found. For values of r lower than r_{crit} the stationary interface approach leads to quicker dissolution of the particle. This is shown in Equation 11 and Equation 12.

$$-\frac{3}{r_{crit}^2} = -\frac{9\,R_0^2}{r_{crit}^4} \qquad \textit{(Equation 11)}$$

$$r_{crit} = \sqrt{3\,R_0^2} = R_0\sqrt{3} \qquad \textit{(Equation 12)}$$

As Equation 12 states, this critical value is always higher than the initial particle radius R_0 as the square root of 3 is greater than 1. This shows that from the beginning,the stationary interface approach will already lead to faster dissolution of the particle than a moving interface approach, given the concentration profile would be the same. This assumption is not entirely correct, as a moving interface would lead to slightly different concentration profiles around the particle, but for further comparison of the models in this work, equal concentration fields are assumed. To grasp the magnitude of difference between the two models, log(Δγ) is plotted in FIG 5 over the particle radius. At the initial particle radius R_0 the difference is 0 as $\gamma_M=\gamma_S$ for $r=R_0$. As the particle dissolves, log(Δγ) grows rapidly at first, but soon the difference between the two modeling approaches somewhat stabilizes for the central part of the dissolution. Only towards the end of the dissolution process, a massive increase in difference between γ_M and γ_S can be observed. To locate the radius at which Δγ starts to increase more rapidly, the second derivative of log(Δγ) can be set to 0 for calculating r_{POI}, which represents the point of inflection of the function. This is done in Equation 13 and Equation 14.

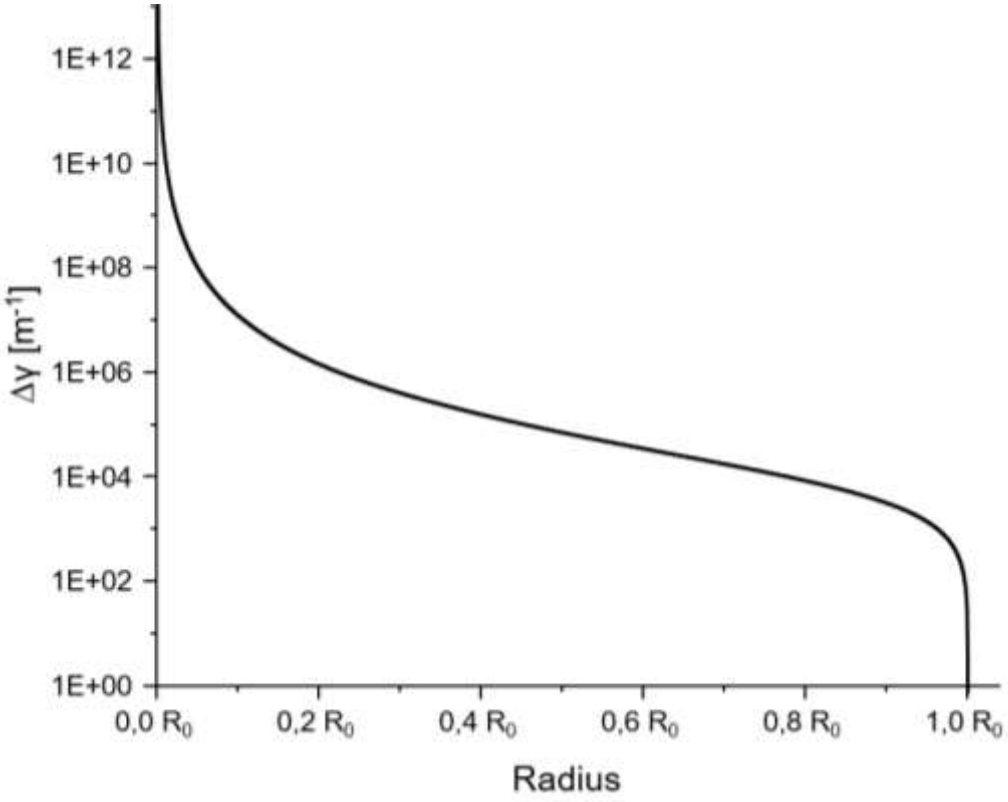

FIG 5 - Δγ plotted over Particle radius

If Equation 14 is solved for r_{POI}, only one solution is positive and smaller than R_0. Only this solution presented in Equation 15 represents the point of inflection for the section of the function of log(Δγ) depicted in FIG 5. This shows that Δγ begins to grow faster as soon as a particle diameter of approximately 63% of R_0 is reached. For an initial radius of R_0 = 250 µm as used for the calculations and HT-CSLM experiments presented in this paper, this leads to r_{POI} = 157 µm or D_{POI}=314 µm, respectively. In FIG 6 this value is marked as a horizontal line. Beyond this point in calculation, the deviation from the experimental results begins to increase rapidly, but before that the simulation is in good agreement to the experimental data.

$$\log_{10}(\Delta\gamma) = \log_{10}\left(\frac{3\,R_0^2}{r_{POI}^3} - \frac{3}{r_{POI}}\right) \qquad \textit{(Equation 13)}$$

$$\frac{d^2}{dr^2}(\log_{10}(\Delta\gamma)) = \frac{r_{POI}^4 - 8r_{POI}^2R_0^2 + 3R_0^4}{\left(r_{POI}^3 - r_{POI}R_0^2\right)^2} = 0 \qquad \textit{(Equation 14)}$$

$$r_{POI} = R_0\sqrt{(4-\sqrt{13})} \cong R_0 * 0.628 \qquad \textit{(Equation 15)}$$

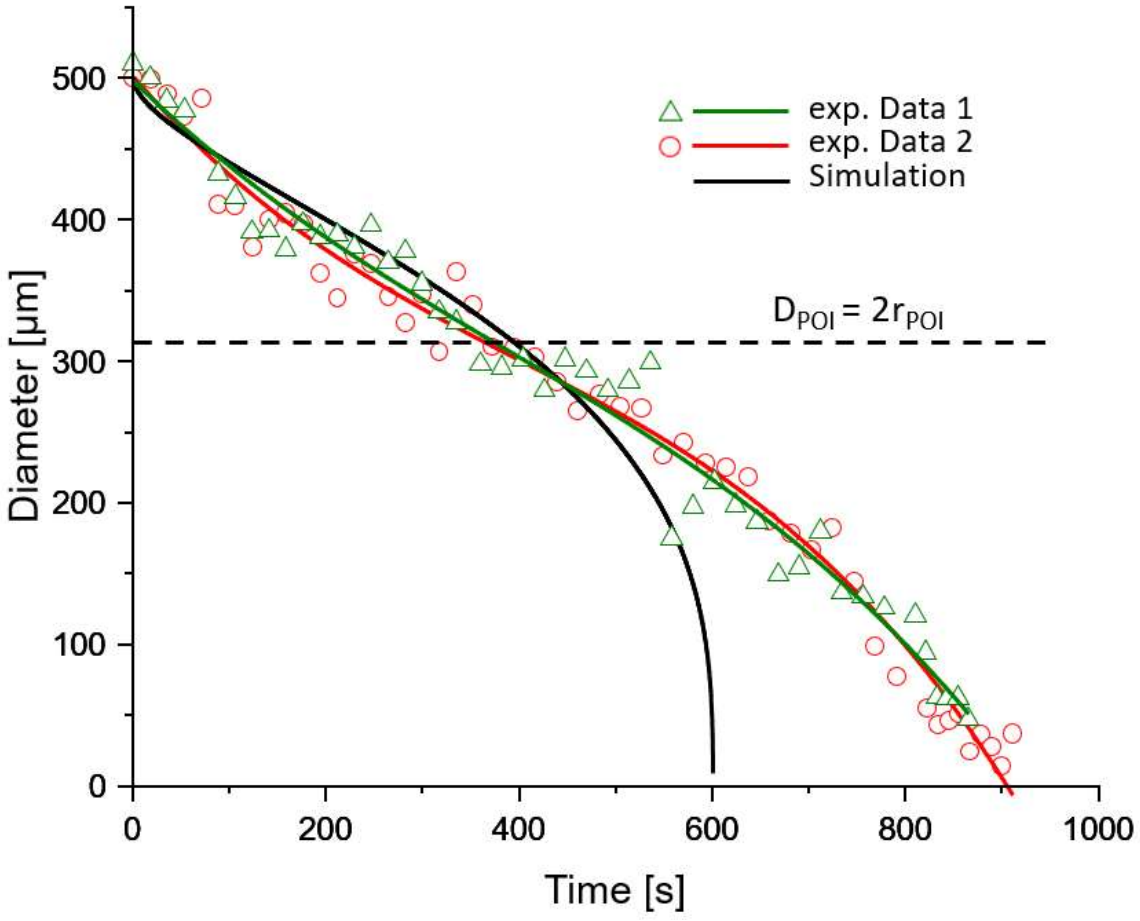

FIG 6 - Comparison of simulation and experimental data. The dashed line represents the diameter of the point of inflection of function log(Δγ).

CONCLUSION

Following these observations, it is proposed to expand the presented model to a moving interface approach as to better predict particle dissolution even at later stages of the dissolution. Additionally, the prediction of dissolution time could improve due to the implementation of more accurate density data of the slag and the dissolving particle. Furthermore, experiments for measuring boundary layer thickness around dissolving particles are of great interest as this is one of the most influential parameters apart from the diffusion coefficient. Once the adapted model is validated by further

experimental data, the prediction of binary diffusion coefficients based on fitting the simulation data to experimental dissolution curves could be possible.

ACKNOWLEDGEMENTS

The financial support by the Austrian Federal Ministry for Labour and Economy, the National Foundation for Research, Technology and Development and the Christian Doppler Research Association is gratefully acknowledged. The authors declare no conflict of interest.

REFERENCES

Burhanuddin,B, Guarco, J, Harmuth, H and Vollmann, S, 2022. Application of an improved testing device for the study of alumina dissolution in silicate slag, Journal of the European Ceramic Society, 8:3652–3659.

Chen, C, Jiang, Z, Li, Y, Zheng, L, Huang, X, Yang, G, Sun, M, Chen, K, Yang, H, Hu, H and Li, H, 2019. State of the Art in the Control of Inclusions in Tire Cord Steels and Saw Wire Steels – A Review, STEEL RES INT, 8:1800547.

Feichtinger, S, Michelic, S K, Kang, Y-B and Bernhard, C, 2014. In-situ observation of the dissolution of SiO_2 particles in $CaO{-}Al_2O_3{-}SiO_2$ slags and mathematical analysis of its dissolution pattern, Journal of the American Ceramic Society, 1:316–325.

Furuya, Y, Abe, T and Matsuoka, S, 2003. 1010-cycle fatigue properties of 1800 MPa-class JIS-SUP7 spring steel, Fatigue & Fracture of Engineering Materials & Structures, 7:641–645.

Garrison, W. M. and Wojcieszynski, A L, 2007. A discussion of the effect of inclusion volume fraction on the toughness of steel, Materials Science and Engineering: A, 1-2:321–329.

Guo, X, Sietsma, J, Yang, Y, Sun, Z and Guo, M, 2017. Diffusion-limited dissolution of spherical particles: A critical evaluation and applications of approximate solutions, AIChE J, 7:2926–2934.

Huo, Y, Gu, H, Huang, A, Ma, B, Chen, L, Li, G and Li, Y, 2022. Characterization and mechanism of dissolution behavior of Al2O3/MgO oxides in molten slags, J. Iron Steel Res. Int., 11:1711–1722.

Jimbo I, Chung Y and Cramb A W, 1996. Interfacial Tensions of Liquid Iron-alloys and Commercial Steels in Contact with Liquid Slags, ISIJ Int., Supplement:S42-S45.

Lee, S H, Tse, C, Yi, K W, Misra, P, Chevrier, V, Orrling, C, Sridhar, S and Cramb, A W, 2001. Separation and dissolution of Al2O3 inclusions at slag - metal interfaces, Journal of Non-Crystalline Solids, 41–48.

Levenspiel, O, 1999. Chemical reaction engineering, pp 582-586 (John Wiley & Sons: New York).

Glicksman, M O, 2000. Diffusion in Solids, p 142 (John Wiley & Sons: New York).

Michelic, S K, Goriupp, J, Feichtinger, S, Kang, Y-B, Bernhard, C and Schenk, J, 2016. Study on Oxide Inclusion Dissolution in Secondary Steelmaking Slags using High Temperature Confocal Scanning Laser Microscopy, Steel Research International, 1:57–67.

Ogris, D M and Gamsjäger, E, 2022. Numerical Treatment of Oxide Particle Dissolution in Multicomponent Slags with Local Gibbs Energy Minimization, STEEL RES INT, 2200056.

Sridhar, S and Cramb, A, 2003. Properties of Slags and Their Importance, in Manufacturing Clean Steels, High Temperature Materials and Processes, 5-6:275–282.

Valdez, M, Shannon, G S and Sridhar, S, 2006. The ability of slags to absorb solid oxide inclusions, ISIJ International, 3:450–457.